# PHRI Safety Control Using a Virtual Flexible Joint Approach

Joseph Diab, Aïcha Fonte, Gérard Poisson, Cyril Novales

# PHRI Safety Control Using a Virtual Flexible Joint Approach

J. DIAB[1], A. FONTE[1] , *, G. POISSON[1] and C. NOVALES[1]
[1]*Laboratoire PRISMES, Université d'Orléans, 8 rue Léonard de Vinci-45072, Orléans, France*
*{joseph.diab, aicha.fonte, gerard.poisson, cyril.novales }@univ-orleans.fr*

Keywords: Physical Human-Robot Interaction, virtual adjustable stiffness, articulation flexibility control.

Abstract: Physical Human-Robot Interaction (PHRI) emphasize on human safety. In literature, two techniques were presented to improving this critical factor concerning moving devices; the first solution is purely mechanical, while the second one is based on the control. In this paper, we describe a new approach combining the two previous solutions. Our proposed paper explores a control scheme involving the use of a virtual component with an adjustable stiffness supposed to be placed between the motor shaft and the robot link. This scheme proposes a Variable Impedance Actuator (VIA) robot control methodology based on the integration of a virtual component, reflecting the behaviour of a real intrinsic Series Elastic Actuator (SEA). This novel method is potentially beneficial in reducing injuries in human/robot interaction by combining a mechanical operating principle and a control approach in order to reduce the collision forces in collaborative applications. This proposed approach was simulated and validated using a UR3 robot model, showing great capacities in reducing collision's peak forces. This paper begins with particular attention to the robot dynamics, then the articulation flexibility and force estimation have been tackled and finally ending the control architecture.

## 1 INTRODUCTION

The presence of unknown obstacles and unpredictable human presence in the modern robotic application implies the usages of more sophisticated control strategies not based only on position control, but a control strategy which allows some degree of flexibility to avoid physical collisions. The nature of those proximate physical interactions is classified into five classes (République Francaise 2017) Those classes can have an unconstraint or constraint impact as a primary source of collision with detailed injury severity description found in ISO/TS 15066 (Sami Haddadin 2008). Reducing personal injuries leads to the spread of flexible articulated robots with SEA or VIA as the primary type of actuator. What separates the SEA and VIA is impedance adjustability. SEA uses active control strategies, like force control, admittance or impedance control, while conserving the joint mechanical properties (Navarro et al. 2018),(Ansarieshlaghi and Eberhard 2019),(Schüthe, Wenk, and Frese 2016),,(Zeng and Hemami 1997), (Pratt and Williamson 1995), opposing to the VIA, which changes its behavioural properties like stiffness and damping to ensure expected joint flexibility (Vanderborght et al. 2013), (Tonietti, Schiavi, and Bicchi 2005), (Lenzi et al. 2011),(Forget et al. 2018), (Spong 1987).

Furthermore, typical collision detection strategies use visual feedback and global interpretation of the working environment to predict the possibility of the probable unwanted interaction (Morikawa et al. 2007), (Kagami et al. 2003), (Ebert and Henrich 2002). In order to achieve a complete knowledge of the environment in robotics applications, a new data type is added to the visual feedback representing the external forces and torques. These forces and torques could be estimated from the movement and the dynamics of the robot, or, for better accuracy, they could be measured by a force sensor located on the end effector.

By acquiring both data feedback, modern robotic has accomplished more advanced tasks and lead to human-robot collaboration in the industry without the need for separation bars.

The novel structure of data highlighted the necessity of force control. Force control in robotics date back to 60th (Whitney 1985), (Maples and Becker 1986); hence it is well defined. This control strategy incorporates the assumption of rigid-body mechanics and assumes a rigid robot with rigid links and joints, even if the current trend is towards soft

robots or robots with flexible articulations or links. The compliance, in this case, could be achieved by one of these following control strategies: Impedance Control, Admittance Control, or Flexible Joints (Bruno and Khatib 2013), (Bissell 2009).

This work focuses on the compliance by the third type control strategies. There are two approaches in order to introduce the flexibility in robot joint: the first one uses the intrinsic mechanical approach with passive safety built in the joint mechanics (Tonietti, Schiavi, and Bicchi 2005), (Sebastián Arévalo et al. 2019), and the second one based fundamentally on the control (De Luca et al. 2006), (Navarro et al. 2016). In literature, joint flexibility was modelled as spring (often linear one) connecting the motor shaft and the following link (Spong 1987), and only a few papers relating to Force/Torque control for this model. Our approach is to keep the usage of the real robot's mechanics but to bring virtual joint flexibility in the control loop in order to mimic the behaviour of a real flexible joint, providing the rigid robot with some degrees of flexibility. This introduced component is here a nonlinear torsional spring located between the geared motor and robot links. The virtual aspect of this coupling can make it possible to modify the mechanical characteristics of the component as required, while it is impossible to modify the mechanical characteristics of a real joint. The control by virtual joint provides then a nonlinear stiffness, and a variable stiffness trajectory representation, given it more adaptability, not like a fixed mechanical device that retains the same stiffness response.

## 2 ROBOT MODEL

In our study, we used a 6 degrees of freedom (DOF) collaborative robot, the UR3 from Universal Robots. Those DOF refer to the number of rotational joints, modelled using modified Denavit–Hartenberg (DH) representation or known as Khalil representation (Khalil and Kleinfinger n.d.) "Table 1".

From "Table 1," the kinematic model of the rigid robot is extracted. The transition from the kinematic model to the dynamic one needs multiple parameters as the link masses and centre of inertia positions; those criteria are located in the robot datasheet (https://www.universal-robots.com/how-tos-and-faqs/faq/ur-faq/parameters-for-calculations-of-kinematics-and-dynamics-45257/ n.d.). Once all parameters are located, the dynamic robot model was obtained through the Lagrange derivation method. We used this one in favour of its practicality in the extraction of robot dynamic symbolic equations (simple derivation of system kinetic and potential energy), comparing it to the recursive Newton-Euler approach. The above method provided the mathematical representation of the UR3's articulated mechanism(Kufieta 2014). This model has completed afterwards with the UR3 motors modelling.

Table 1: UR3 MODIFIED DH TABLE (RAD AND MM).

| joints | Table Column Head (rad and mm) | | | | |
|---|---|---|---|---|---|
| | $\sigma_i$ | $\alpha_{i-1}$ | $a_{i-1}$ | $\theta_i$ | $r_i$ |
| 1 | 0 | 0 | 0 | $\theta_1$ | -248.1 |
| 2 | 0 | $-\pi/2$ | 0 | $\theta_2$ | 0 |
| 3 | 0 | 0 | 243.65 | $\theta_3$ | 0 |
| 4 | 0 | 0 | 213.25 | $\theta_4$ | 112.35 |
| 5 | 0 | $-\pi/2$ | 0 | $\theta_5$ | 85.35 |
| 6 | 0 | $\pi/2$ | 0 | $\theta_6$ | 81.9 |

The used UR3 was developed for light assembly tasks and direct physical cooperation with humans with a payload not exceeding 30N. This robot has ±360° of rotational wrists and an infinite end-effector rotational joint. Its maximum extended arm reaches 500 mm.

Since the workspace is a joint space, the canonical equation of the robot dynamics is formulated by the following:

$$M(q)\ddot{q} + C(q,\dot{q})\dot{q} + g(q) = \tau + \tau_{ext} \qquad (1)$$

Where M(q), C(q,q˙ ), g(q), τ, and τ_ext represent robot inertia matrix, Coriolis force matrix, robot links gravitational force vector, joint actuation torques, and the external joint torques.

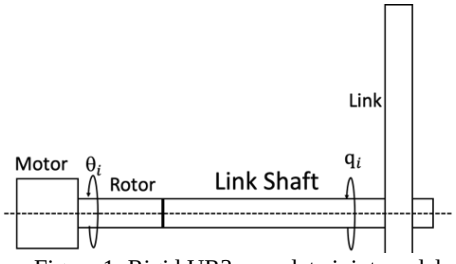

Figure 1: Rigid UR3 complete joint model.

"Equation_1" does not take in consideration the effects of the motor on the robot dynamics; the

enhanced formulation of this equation could be presented by the following:

$$H(q)\begin{pmatrix}\ddot{q}\\ \ddot{\theta}\end{pmatrix} + \Gamma(q,\dot{q})\dot{q} + g(q) = \begin{pmatrix}\tau + \tau_{ext}\\ \tau_m\end{pmatrix} \qquad (2)$$

Where $H(q)$, $\Gamma(q,\dot{q})$ and $\tau_m$represent the global inertia matrix, global Coriolis force matrix, and the motor torques.

"Equation_2" assumes that the robot link is directly connected to the motor shaft, as shown in "Figure 1".

The extracted model presented in "Equation_1" and "Equation_2" is rigid and do not allow any compliance or any movement between the motor shaft and robot link, to ensure a compliance behaviour in such system joint flexibility must be integrated into the model to vary joints rigidities.

# 3 JOINT FLEXIBILITY

Without taking into account the mechanical reversibility introduced in the mechanical field as variable-stiffness transmission (Nelson, Nouaille, and Poisson 2019). "Figure 1" and "Equation_2" presents a rigid model without any flexible part between the rotor shaft and the robot link. This model does not allow any compliance in case of a collision or human interaction. To solve this problem, "Equation_2" could integrate a new term to allow such motion.

The joint flexibility in this context is provided by a virtual flexible joint, with a nonlinear spring supposed to be located between the rotor and the link similar to "Figure 2". The virtual spring, once provided with the motor and robot joint angular position, produces the correspondent torque needed by the robot.

In order to adapt "Equation_2", Spong's assumption must be respected: 1. The kinetic energy of the rotor is due mainly to its rotation, 2. The rotor/gear inertia is symmetric about the rotor rotation axis (Spong 1987). Motor electrical dynamic (i.e., feedback current in the control loop) was neglected, with the assumption that the electric system time constant is much smaller than the mechanical one.

The newly implemented spring introduces a new term in system potential energy. Therefore, the potential energy is divided into two parts:

- The old gravity potential of "Equation_2".
- The stiffness potential $V_k$ (Radomirovic and Kovacic 2013).

$$V_k(q,\theta) = \sum_{i=1}^{n} V_{K,i}(q_i,\theta_i) \qquad (3)$$

$$V_{K,i}(q_i,\theta_i) = \int_0^{\theta_i - q_i} f(\theta_i,q_i)\, d(\theta_i - q_i) \qquad (4)$$

Where f(θi, qi), is a nonlinear function expressing the spring torque in the function of spring deflection (θi-qi).

The derivation of "Equation_3" respectively to θ and q and its reintroduction in the "Equation_2" gives:

$$H(q)\begin{pmatrix}\ddot{q}\\ \ddot{\theta}\end{pmatrix} + \Gamma(q,\dot{q})\dot{q} + \begin{pmatrix}g(q) - \mathrm{F}(\theta,\mathrm{q})\\ \mathrm{F}(\theta,\mathrm{q})\end{pmatrix} = \begin{pmatrix}\tau_{ext}\\ \tau_m\end{pmatrix} \qquad (5)$$

Where F(θ, q) is nonlinear spring torque vector with:

$$\mathrm{F}(\theta,\mathrm{q}) = \begin{pmatrix} f(\theta_i,q_i)\\ \dots\\ f(\theta_n,q_n)\end{pmatrix} \qquad (6)$$

While colliding into an obstacle, the deflection angle (θ-q) becomes increasingly significant. The gape introduced between rotors and links angular positions, as shown in "Figure 2", requests the stiffness coefficient of f(θi, qi) to be adjusted.

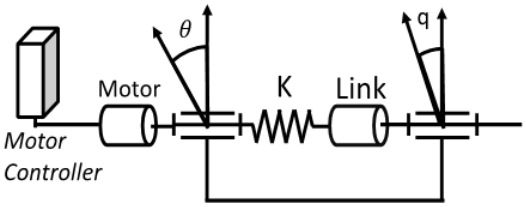

Figure 2: Flexible joint.

The stiffness of nonlinear spring is given by:

$$K_i = \frac{df(\theta_i,q_i)}{d(\theta_i - q_i)} \qquad (7)$$

The reduced form of the "Equation_5" can be written according to (De Luca et al. 2006), (Martinoli et al. 2012) by the following:

$$M(q)\ddot{q} + C(q,\dot{q}) + g(q) = \mathrm{F}(\theta,\mathrm{q}) + \tau_{ext} \qquad (8)$$

$$B\ddot{\theta} + \mathrm{F}(\theta,\mathrm{q}) = \tau_m \qquad (9)$$

Where B is the rotors inertia matrix.

f(θi, qi) could be a constant, decreasing, or increasing, linear, or nonlinear function. This wide

variety of choices is not applicable in the flexible mechanical joint due to the limitation in the adjustability of the mechanical component. As a result, the function f(θi, qi) has to provide a suitable torque to the links in all cases (colliding or not).

Following Spong's definition (Spong 1987) and (Haddadin et al. 2008), f(θi, qi) is given by an equation which respects Hook's Law:

$$f(\theta_i, q_i) = K * (\theta_i - q_i) \quad (10)$$

Where K, is a fixed spring stiffness coefficient. With a small sampling time, the local zone of nonlinear spring has similar behaviour to Hook's law presented in the "Equation_10". Consequently, the simulated nonlinear spring could be defined as linear spring with variable stiffness K.

In this paper, K is ranged between two values: Kmin and Kmax, representing respectively the minimum and maximum spring's stiffness. In the absence of collision, K equals Kmax, but while colliding, K degenerates rapidly until Kmin. To be able to distinguish one case from another, a trigger should be integrated into the selection of K. The deflection angle (θi-qi) is used for this purpose. The value of (θi-qi) < ~0.0873 rad is used as a threshold to activate K, as shown in "Figure 3". Kmax is different for each articulation because it depends on the maximal torque of each UR3's motors varying between 12 Nm and 56 Nm.

"Figure 3" is used to illustrate a trajectory of K, with Kmax=100 Nm/rad

K is defined as the following:

$$K = \begin{cases} K_{max}\ ;\ \text{if } (\theta - q) < \sim 0.0873 rad \\ K_{min} * \sin(4(\theta - q)) + K_{max} * \cos(3(\theta - q)) \\ K_{min}\ ;\ \text{if } (\theta - q) > \sim 0.5236 \text{rad} \end{cases} \quad (11)$$

"Equation_11" uses a combination of sin and cos to insure a fast degeneration of K when 5°< θ-q <30°.

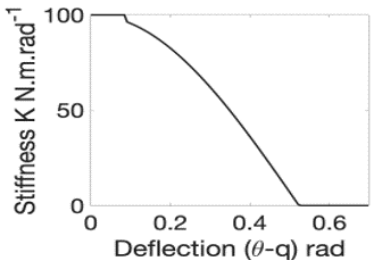


Figure 3: Spring stiffness K, with Kmin=0.001 Nm/rad, Kmax=100 Nm/rad.

In order to control the new flexible robot, external torques should be introduced into the robot dynamics "Equation_8". The simplest way to introduce those requirements is to estimate those parameters.

# 4 FORCE ESTIMATION

The transmitted torques between the simulated robot and the trajectory generation subsystem shown in "Figure 4" are easily measured on UR3. Those measurements are possible because of UR3 associates torque sensors in its articulation. Those torques were taken into account using the robot model "Equation_1".

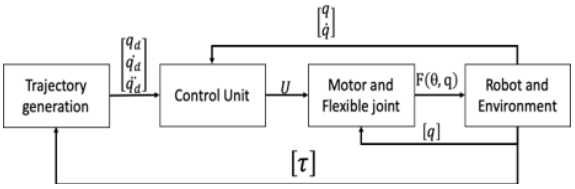


Figure 4: The control architecture.

The external joint torques $\tau_{ext}$ according to (De Luca and Mattone 2005), is coupled to the generalized contact force Fext by:

$$\tau_{ext} = J^T * F_{ext} \quad (12)$$

"Equation_12" adopt the knowledge of external forces applied on the end-effector in the contact point with the object, those external contact forces were obtained in our case by a linear spring-damper model to estimate or simulate $F_{ext}$ . Those reaction forces are then calculated afterwards according to the end effector penetration depth and velocity. For this purpose, the object position could be extracted from image processing algorithms (Collet et al. 2009), but in this study, it was supposed located in a fixed, known Cartesian frame [x,y,z].

The calculated reaction forces are based on linear spring-damper contact mechanism model given by:

$$F_{ext} = -K_s * X_{pen} - * sign(X_{pen}) * D * V_{pen} \quad (13)$$

Where Ks is the spring stiffness, Xpen is the difference between the robot end-effector Cartesian position and the object position, D and Vpen=ΔXpen/Δt, are respectively, the spring damping coefficient and the speed of end-effector penetration.

"Equation_12" and "Equation_13" construct the first external force/torque estimator. This torque is added subsequently to the joint torques calculated using the dynamic robot model. The combined torques provide the complete joint torque, used as an input to the trajectory generation subsystem, where the second torque estimator is located.

The 6th order polynomial trajectory generator "Figure 5" ensures a smooth trajectory, with a smooth high order derivative, resulting in consideration of the equality in the desired and the real articulation position. This assumption leads to a newer description of robot dynamics using the desired positions and their derivatives.

From all the above, a second torque observer can be derived from the desired positions. This torque observer represents the expected joint torques in a collision-free environment regarding the desired trajectory. Introducing those assumptions in "Equation_1" gives:

$$\hat{\tau} = \widehat{M}(q_d)\ddot{q_d} + \hat{C}(q_d, \dot{q}_d) + \hat{g}(q_d) \qquad (14)$$

In the absence of collision, "Equation_1" is identical to "Equation_14". This equality promotes the extraction of the estimated external torque presented in "Equation_15".

$$\widetilde{\tau_{ext}} \approx \tau_{ext} = \tau - \hat{\tau} \qquad (15)$$

The first estimator provides the simulation with the external forces and torques undergo by the end effector, while the output of the second estimator can alter the robot trajectory.

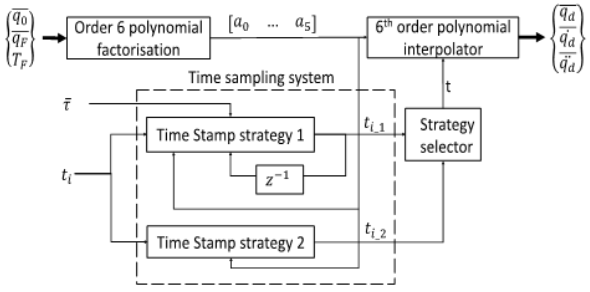

Figure 5: Trajectory generation subsystem.

The estimated external torques are crucial factors in the control architecture and the trajectory generation because they indicate the variation of joint torques before and upon a collision. This identified variation can be a trigger to change robot motion in control architecture.

# 5 CONTROL ARCHITECTURE

The architecture of the complete system is divided into four subsystems: (1) Trajectory generation, (2) Control Unit, (3) Motor and Flexible joint, (4) Robot and Environment see "Figure 4".

Trajectory generation subsystem takes a destination in the articulation space with a starting and ending time, and generate a smooth trajectory from the reference to the desired position.

The primary role of the Control Unit subsystem is to compensate for system errors. Those errors contain gravitation, Coriolis/centrifugal forces, and position. We used a feedforward combined with a PD controller to generate a torque command U for the motor model (De Luca 2000).

The robot and environment subsystem combine the simulated robot and its interaction effects on the simulated body (i.e., fixe object).

Referring to "Equation_8", our dynamic model is a nonlinear system, and therefore in order to control such a mechanism, a nonlinear control approach must be used.

To preserve robot articulation and to ensure a displacement without stepping, robot trajectory must be smooth without any discontinuities in its movement, velocity, or acceleration. In addition to previous constraints, the robot displacement must obey a finale delay to accomplish a predefined task. Those above conditions render the trajectory generation a time-dependent problem. Thus, an interpolation method needed in order to link space and time.

The trajectory generation subsystem in "Figure 5", relays on time scaling to generate the appropriate desired trajectory using sixth-order polynomial interpolation.

Discrete-time $t_i$ , is written as $t_i = t_{i-1} + \Delta t$, regarding Δt, the discrete sampling time. To combine space and time vector, we need to redefine our interpolation time in order to change the trajectory upon an undesired collision. This task is provided by the time sampling system, which feeds the strategy selector with two current times $t_{i_1}$ and $t_{i_2}$. $t_{i_1}$ is a modified time implicitly integrating the estimated joints torques $\tilde{\tau}$.

$t_{i_1}$ is given by the equation below:

$$t_{i_1} = \begin{cases} t_{mod_{i-1}} + fs\left(g(\widetilde{\tau_{ext}})\right) * \Delta t \;\; ; \; t_{i_1} < T_F \\ T_F \;\; ; \;\; t_{i_1} \geq T_F \end{cases} \qquad (16)$$

Where $fs(g(\widetilde{\tau_{ext}}))$ is a function outputting 0 or 1 considering a threshold for the mapped estimated external torques $g(\widetilde{\tau_{ext}})$.

$$fs(g(\widetilde{\tau_{ext}})) = \begin{cases} 1 & ; \ |g(\widetilde{\tau_{ext}})| < 0.2 \\ 0 & ; \ |g(\widetilde{\tau_{ext}})| \geq 0.2 \end{cases} \quad (17)$$

$g(\widetilde{\tau_{ext}})$ takes the estimated external torques $\widetilde{\tau_{ext}}$ deduced by the torque estimator and produces a value ranging between [0,1] representing the relation between the estimated torque and the maximum motors torques.

$$g(\widetilde{\tau_{ext}}) = \frac{(\widetilde{\tau_{ext}} - \tau_{m_{min}})}{(\tau_{m_{max}} - \tau_{m_{min}})} \quad (18)$$

$t_{i_2}$ is given by "Equation_19":

$$t_{i_2} = \begin{cases} t_i & ; \ t_i < T_F \\ T_F & ; \ t_i \geq T_F \end{cases} \quad (19)$$

$t_{i_1}$ of "Equation_16" and $t_{i_2}$ of "Equation_19" are fed to the strategy selector, which compares $t_{i_1}$ and $t_{i_2}$, if those two are equals that means no collision is detected, then the selection is made to take $t_{i_2}$ as an interpolation time, in case of difference $t_{i_1}$ is selected. In collision $t_{i_1}$ is always constant equals to the time before the collision. This constant time implies a constant trajectory during and after the impact.

For illustration and presentation purposes, the simulation results of the complete system are presented in the following part.

# 6 SIMULATION RESULTS

The simulation of the collision detection and compliance strategy was performed with robotics conditions under gravitational force. The joint positions were expected to be obtained by digital encoders.

All joints velocities and accelerations were acquired in two ways by numerical differentiation or by numerical computation. Those mathematical operations introduce a certain level of realistic noise in the simulation.

The trajectory is generated between $q_0$ and $q_f$, representing two $R^n$ vectors with n=6. Where $q_0$ is the initial starting joint robot positions at $T_i = 0\ s$ and $q_f$ is the ending joint position at $T_F = 2\ s$. The desired articulations positions according to the two strategies of "Figure 5" can be observed in "Figure 6".

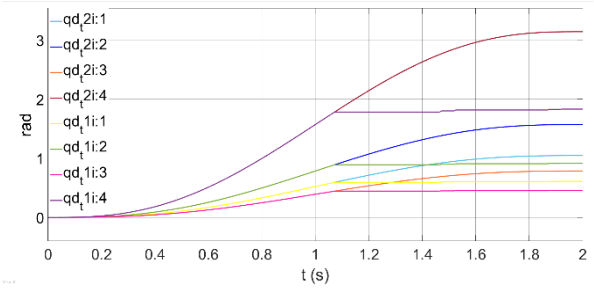


Figure 6: Trajectory deformation.

The deformation of the desired trajectory at t=1.08s, as shown in "Figure 6", helps to stop the robot upon a collision. The strategy selector, represented in "Figure 5", switches the interpolation time from $t_{i_2}$ to $t_{i_1}$, causing the time t to be constant $t = t_{collision}$. As a result, the Feedforward system maintains fixed torque values until the obstacle is removed, or the contact between human-robot has evolved (eg. pushing on the robot or evading the contact).

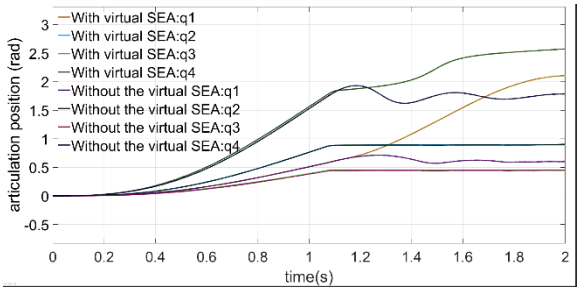


Figure 7: Difference in articulation positions between system 1: with the virtual SEA and system 2: without the flexible components. It is illustrated on the first four axes of the robot. Here q1 and q4 are the only ones impacted by the strategy.

"Figure 7" shows the comparison of the robot articulations positions between a system integrating the virtual SEA and another without it.

The compliance in "Figure 7" is shown by the increase of angular position of q1 and q4. This angular growth is a response to the increase in joint flexibility.

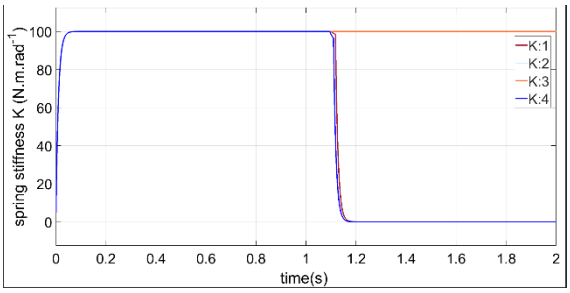


Figure 8: Spring stiffness, K.

"Figure 8" introduces the behaviors of the virtual SEA in four regions, [0s, 0.2s], [0.2s, 1.08s], [1.08s, 1.2s] and [1.2s, 2s]. In these regions, the stiffness of the springs varies; they increase in the first region, until saturation with a maximale stiffness (Kmax) in the second region, towards a rapid decrease during the collision, and finally, they maintain a constant value of the minimale stiffness (Kmin) after the collision.

The deflection angle $(\theta - q)$ causes the variation in K. In the first zone $(\theta - q)$ decreases because in this zone, rotors positions were following a fixed reference $q = q_d$. The saturation of K in the second zone happened when the rotor and joint angular differences are less than 0.0873 rad (about 5°). The stiffness decreases in zone 3, due to the increase of angular difference $(\theta - q)$. This zone represents the collision zone, where the trajectory is modified, as shown in "Figure 6". The fixed trajectory implies a fixe rotor angle, which is the leading cause of the expansion of the gap between $(\theta - q)$ shown in "Figure 2". In this case, the variation of q is induced by Kmin nullifying torques values to the affected joint. Rendering torques to 0 results in vast freedom of movement of the joint. This freedom is highlighted in the end zone, where K is fixed as Kmin.

"Figure 8" illustrates the trajectory issued from "Equation_11", and shows the effects of the articulation flexibility on altering the joint trajectory. The new trajectory generated by the flexible joint has a direct effect on the forces between the end-effector and the object. Those effects are shown in the following figure, "Figure 9".

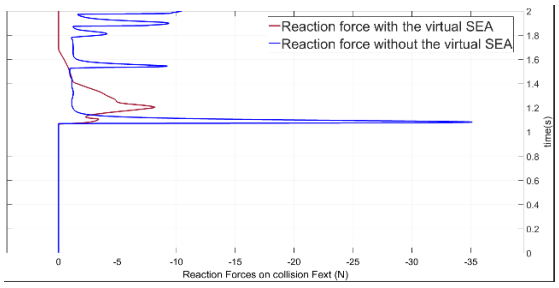


Figure 9: The difference in reaction forces between the 2 systems.

"Figure 9" indicates the reduction of peak force values on the impact. The variation of joint flexibility shown in "Figure 8", induced changes on the Cartesian positions of the end-effector, this variation leads to a new penetration value for "Equation_13"; the joint flexibility induced by the virtual SEA insure a smaller value of penetration for the first force estimator giving in overall smaller reaction forces and torques. "Figure 9" shows the main difference between the two systems, the first one with the variable stiffness (the red line) reduced the value of reaction force to 0 at t=1.6s, while the second system stiffness (the blue line) is oscillating with much higher contact forces. The virtual SEA gives the robot, in this case, the flexibility to move away from the collision case.

# 7 COMPARATIVE DISCUSSIONS

From above, there is a two way to implement compliance in a robotic using VIA or SEA systems. Each type of those induced flexibilities holds advantages and drawbacks.

In the case of SEA, robot compliance is ensured by the control architecture. The controller varies the actuation torque to reshape the desired path. Contrary to VIA, SEA needs the presence of force/torque sensors to trigger collision detection and re-evaluation of the trajectory.

In other words, VIA acts directly on the path while SAE needs a control loop to make a path change.

Our approach combines the two above methods by adding the VIA virtual component to the existing SAE control loop, ensuring additional compliance in the event of a collision, this additional layer makes the robot softer in the event of a crash. It permits the reduction of impact forces compared to the two previous methods.

SEA benefits from active compliance induced by an active controller which complexify the implementation of such a solution. While VIA, due to its passive compliance, does not need a complex control scheme, facilitating its implementation in a robotic application. Our solution, as mentioned before, is the combination of both systems, which gives this solution the benefice of the active control scheme and virtual passive flexibility.

This approach makes the proposed compliance more adjustable from the ordinary SEA controller,

and more controllable and reliable than a passive VIA.

Due to the uprising of COVID-19 pandemic, the planned experiments in the laboratory on the robot have been impossible to perform. We, therefore, stayed on simulations. This way provides us with enough data to be interpreted and brings promising answers for the future validation on a real robot.

Fist, the simulated experiment was conducted to highlight and to accentuate on the advantages of our approach. This simulation concerns two cases: case "A" showing pure SEA behaviour and case "B" presenting the proposed solution. In "A", the robot (a UR3 from Universal Robots) is supposed to be controlled using an impedance controller, while in "B", the robot is subjected to the same controller of "A" plus a virtual VIA. In all experiments, a wall is also supposed to be located at the proximity of the robot. The wall is placed in a way that ensures a collision with the moving the robot arm. In those simulations, we will compare the insertion of the robot end-effector into the wall, the force upon and after the collision.

The robot's configuration on the collision is shown in "Figure 10":

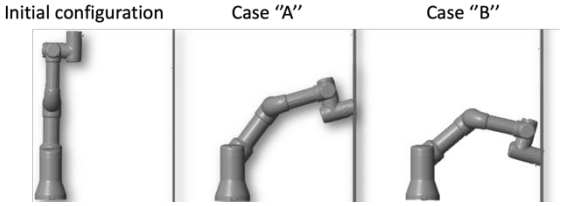


Figure 10: Robot position in multiple configurations near the right wall.

The robot in "A" is controlled with impedance control which tends to stop it on the desired position where the contact point with the wall as shown in "Figure 10".

While in " B", we can notice additional compliance behaviour manifesting by the difference in the configuration of the robot arm, as shown in "Figure 10".

In case "A" and "B" we notice the same behaviour, were the robot kept it end effector on the contact point with the wall.

The difference in the end effector position at the end of the simulation is closely related to the virtual VIA that has been introduced by the nonlinear torsional spring. The figure highlights the role of the stiffness in the flexibility of the articulation where we can notice that the third and second articulation are lower in B than A. This difference is the result of the variation of the actuation torque $f(\theta_i, q_i)$ by adjusting the stiffness in equation 10.

In case of cobotic application maintaining a safe distance in a collision is important, but the main factor affecting the severity of the injury is how much force was applied in the collision and when the robot is stopped. The forces of cases "A" and "B'' are shown in "Figure 11".

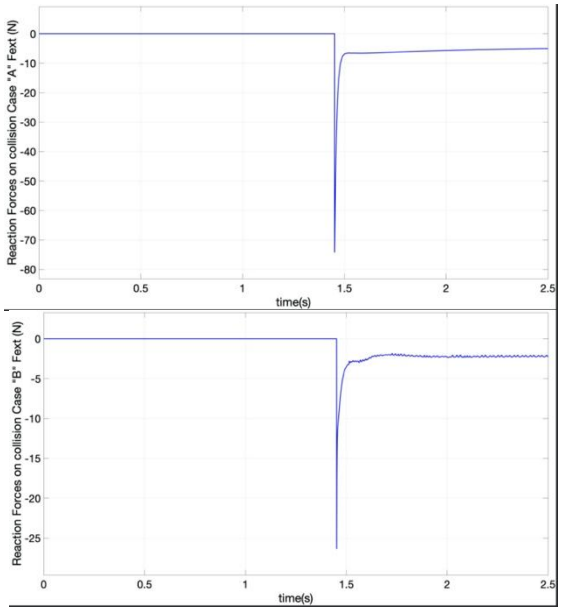


Figure 11: Robot forces upon and after the collision for the case "A" and "B".

"Figure 11" showcase robots end-effector's reaction forces in case "A" and "B", where the maximum impact forces differ from one situation to another. In "A" the maximum impact forces registered a value of 76 N, wherein "B" this value is divided by 3, with maximum values of 26 N.

This difference in force values is not limited to the impact; also an important reduction of its finale values can be noticed, wherein "B" the Fext is around 2 N while in "A" Fext is approximately 8 N.

So in case of collision, the injury in case "A" would be with much higher consequences while in "B" the injury severity would be less.

Those two aspects of the case "B" answer the safety factor of cobotic application, firstly by limiting the robot action and displacement by fixing the robot workspace to the position of the contact limiting the risk of insertion, and by reducing the

contact force, the case “B” also reduces collision damages in cobotics.

# 8 CONCLUSIONS

Concluding, we presented the feasibility of such an integrated virtual SEA and its effect on robot joint displacement without the need for altering the existing robot joint.

The presented method combines the existent VIA and SEA flexibility to produce a compliant robot. The obtained simulation result validates the compliance behaviour and could lead to a more secure robot, which can reduce the stiffness of its joint at any probable human risk, adding in a manner some of the additional degrees of safety to the existent PHRI.

Another advantage of such a system is to adapt the joint stiffness behaviour to suit not only one specific profile but much more complex ones.

This method offers a promising new way of reducing the forces on a collision subject, it is still in development, in particular as for its adaptation to different fields of application.

We intend in the future work to validate the simulation result with experimental data. The next step will be oriented towards applying this new command law on a UR3 integrated into a complex environment. The extracted experimental data will help us to refine this strategy so that it will be safer and more reliable for human-robot interaction.

# ACKNOWLEDGMENTS

This work has been realized as part of an ANR (French National Research Agency) SISCob project ANR-14-CE27-0016.

# REFERENCES

Ansarieshlaghi, Fatemeh, and Peter Eberhard. 2019. “Hybrid Force/Position Control of a Very Flexible Parallel Robot Manipulator in Contact with an Environment.” *ICINCO 2019 - Proceedings of the 16th International Conference on Informatics in Control, Automation and Robotics* 2(Icinco): 59–67.

Bissell, C C. 2009. Springer Handbook of Automation *Springer Handbook of Automation*. ed. Shimon Y. Nof. Berlin, Heidelberg: Springer Berlin Heidelberg. http://link.springer.com/10.1007/978-3-540-78831-7.

Bruno, Siciliano, and Khatib. 2013. 46 Choice Reviews Online *Springer Handbook of Robotics*. eds. Bruno Siciliano and Oussama Khatib. Berlin, Heidelberg: Springer Berlin Heidelberg. http://link.springer.com/10.1007/978-3-540-30301-5.

Collet, Alvaro, Dmitry Berenson, Siddhartha S. Srinivasa, and Dave Ferguson. 2009. “Object Recognition and Full Pose Registration from a Single Image for Robotic Manipulation.” : 48–55.

Ebert, Dirk M., and Dominik D. Henrich. 2002. “Safe Human-Robot-Cooperation: Image-Based Collision Detection for Industrial Robots.” *IEEE International Conference on Intelligent Robots and Systems* 2(October): 1826–31.

Forget, Florent et al. 2018. “Implementation, Identification and Control of an Efficient Electric Actuator for Humanoid Robots.” *ICINCO 2018 - Proceedings of the 15th International Conference on Informatics in Control, Automation and Robotics* 2(Icinco): 29–38.

Haddadin, Sami, Alin Albu-Schäffer, Alessandro De Luca, and Gerd Hirzinger. 2008. “Collision Detection and Reaction: A Contribution to Safe Physical Human-Robot Interaction.” *2008 IEEE/RSJ International Conference on Intelligent Robots and Systems, IROS*: 3356–63.

“Https://Www.Universal-Robots.Com/How-Tos-and-Faqs/Faq/Ur-Faq/Parameters-for-Calculations-of-Kinematics-and-Dynamics-45257/.”

Kagami, Satoshi et al. 2003. “Humanoid Arm Motion Planning Using Stereo Vision and RRT Search.” *IEEE International Conference on Intelligent Robots and Systems* 3(October): 2167–72.

Khalil, W., and J. Kleinfinger. “A New Geometric Notation for Open and Closed-Loop Robots.” In *Proceedings. 1986 IEEE International Conference on Robotics and Automation*, Institute of Electrical and Electronics Engineers, 1174–79. http://ieeexplore.ieee.org/document/1087552/.

Kufieta, Katharina. 2014. “Force Estimation in Robotic Manipulators: Modeling, Simulation and Experiments.” : 144.

Lenzi, Tommaso et al. 2011. “NEUROExos: A Variable Impedance Powered Elbow Exoskeleton.” *Proceedings - IEEE International Conference on Robotics and Automation*: 1419–26.

De Luca, Alessandro. 2000. “Feedforward/Feedback Laws for the Control of Flexible Robots.” *Proceedings - IEEE International Conference on Robotics and Automation* 1(April): 233–40.

De Luca, Alessandro, Alin Albu-Schäffer, Sami Haddadin, and Gerd Hirzinger. 2006. “Collision Detection and Safe Reaction with the DLR-III Lightweight Manipulator Arm.” *IEEE International Conference on Intelligent Robots and Systems*: 1623–30.

De Luca, Alessandro, and Raffaella Mattone. 2005. “Sensorless Robot Collision Detection and Hybrid Force/Motion Control.” *Proceedings - IEEE International Conference on Robotics and Automation* 2005(April): 999–1004.

Maples, James A., and Joseph J. Becker. 1986. “Experiments in Force Control of Robotic Manipulators.” : 695–702.

Martinoli, Alcherio, Francesco Mondada, Nikolaus Correll, and Grégory Mermoud. 2012. 83 STAR Springer Tracts in Advanced Robotics *Springer Tracts in Advanced Robotics: Preface*.

Morikawa, Sho, Taku Senoo, Akio Namiki, and Masatoshi Ishikawa. 2007. “Realtime Collision Avoidance Using a Robot Manipulator with Light-Weight Small High-Speed Vision Systems.” *Proceedings - IEEE International Conference on Robotics and Automation* (April): 794–99.

Navarro, Benjamin et al. 2016. “An ISO10218-Compliant Adaptive Damping Controller for Safe Physical Human-Robot Interaction.” *Proceedings - IEEE International Conference on Robotics and Automation* 2016-June: 3043–48.

———. 2018. “Physical Human-Robot Interaction with the OpenPHRI Library To Cite This Version : HAL Id : Hal-01823337 Physical Human-Robot Interaction with the OpenPHRI Library Two-Layer Safe Damping Control Framework.”

Nelson, Carl A, Laurence Nouaille, and Gérard Poisson. 2019. 73 *Advances in Mechanism and Machine Science*. Springer International Publishing. http://link.springer.com/10.1007/978-3-030-20131-9.

Pratt, Gill A., and Matthew M. Williamson. 1995. “Series Elastic Actuators.” *IEEE International Conference on Intelligent Robots and Systems* 1: 399–406.

Radomirovic, Dragi, and Ivana Kovacic. 2013. “Deflection and Potential Energy of Linear and Nonlinear Springs: Approximate Expressions in Terms of Generalized Coordinates.” *European Journal of Physics* 34(3): 537–46.

République Francaise. 2017. “Guide de Prévention à Destination Des Fabricants et Des Utilisateurs Pour La Mise En Oeuvre Des Applications Collaboratives Robotisées-Edition 2017.” *Ministère du travail*. https://travail-emploi.gouv.fr/IMG/pdf/guide_de_prevention_25_aout_2017.pdf.

Sami Haddadin, Elizabeth Crof. 2008. “Handbook of Robotics: Physical Human-Robot Interaction.” *Handbook of Robotics*: 1835–74.

Schüthe, Dennis, Felix Wenk, and Udo Frese. 2016. “Dynamics Calibration of a Redundant Flexible Joint Robot Based on Gyroscopes and Encoders.” *ICINCO 2016 - Proceedings of the 13th International Conference on Informatics in Control, Automation and Robotics* 1(Icinco): 335–46.

Sebastián Arévalo, Laribi, Zeghloul, and Arsicault. 2019. “On the Design of a Safe Human-Friendly Teleoperated System for Doppler Sonography.” *Robotics* 8(2): 29.

Spong, M. W. 1987. “Modeling and Control of Elastic Joint Robots.” *Journal of Dynamic Systems, Measurement and Control, Transactions of the ASME* 109(4): 310–19.

Tonietti, Giovanni, Riccardo Schiavi, and Antonio Bicchi. 2005. “Design and Control of a Variable Stiffness Actuator for Safe and Fast Physical Human/Robot Interaction.” *Proceedings - IEEE International Conference on Robotics and Automation* 2005(April): 526–31.

Vanderborght, B. et al. 2013. “Variable Impedance Actuators: A Review.” *Robotics and Autonomous Systems* 61(12): 1601–14. http://dx.doi.org/10.1016/j.robot.2013.06.009.

Whitney, Daniel E. 1985. “Historical Perspective and State of the Art in Robot Force Control.” *Proceedings - IEEE International Conference on Robotics and Automation*: 262–68.

Zeng, Ganwen, and Ahmad Hemami. 1997. “An Overview of Robot Force Control.” *Robotica* 15(5): 473–82.